DOI: 10.1002/ ((please add manuscript number))

Article type: (**Full Paper**)

Title: A two-resonance tapping cavity for an optimal light trapping in thin-film solar cells

Quan Liu,[1] *Pablo Romero-Gomez,*[1] *Paola Mantilla-Perez,*[1] *Silvia Colodrero,*[1] *Johann Toudert,*[1] *and Jordi Martorell*[1, 2*]

[1]ICFO-Institut de Ciencies Fotoniques, The Barcelona Institute of Science and Technology, 08860 Castelldefels (Barcelona), Spain

[2]Departament de Física, Universitat Politècnica de Catalunya, 08222 Terrassa, Spain

[*]Corresponding authors E-mail: jordi.martorell@icfo.es

Keywords: Thin-film solar cell, light trapping, optical cavity, PTB7-Th, Perovskite

Abstract: An optimal photon absorption in thin film photovoltaic technologies can only be reached by effectively trapping the light in the absorber layer provided a considerable portion of the photons are rejected or scattered out of such layer. In here, we propose a new optical cavity that can be made to have a resonant charcter at two different non-harmonic frequencies when adjusting the materials or geometry configurations of the partially transmitting cavity layers. We find specific configurations where a reminiscence of such two fundamental resonances co-exist leading to a broadband light trapping. When a PTB7-Th:$PC_{71}BM$ organic cell is integrated within such cavity, we measure a power conversion efficiency of 11.1%. We also demonstrate that when materials alternative to organics are used in the photoactive cell layer, a similar cavity can be implemented to also obtain the largest light absorption possible. Indeed, when we apply it to perovskite cells we predict an external quantum efficiency that closely matches its corresponding internal one for a broad wavelength range.

1. Introduction

In thin film photovoltaic (PV) technologies as the organic, quantum dot or perovskite based the efficiency in photon absorption remains well below the desirable 100%.[1-4] On average, one may estimate that more than 20% of the photons are scattered out of the device or absorbed outside of the active layer.[5-8] Over decades of thin film technology, many different physical phenomena have been considered and partial success has been reached when a certain degree of light trapping has been demonstrated.[9-10] Solar cells incorporating hexagonal arrays of nano-columns[11-12] or nano-hole[13] embossed in the active layer, nano-imprinted electrode capable of both diffracting light and collecting the photo-generated carriers,[14-15] textured electrodes in a periodic grating[16-17] or in a random configuration,[18] 1-D photonic crystals or Bragg reflectors for semi-transparent cells,[19-24] nanospheres to couple light in the whispering gallery,[25-27] metallic nanoparticles to increase light absorption as well as exciton dissociation,[28-30] nanocubes[31] or oligomers,[32-33] exhibited an improvement relative to a given reference cell. However, light trapping or confinement has never been shown to be critical to achieve record performing thin film cells.

In this paper, we propose a new optical cavity design which can be constructed to exhibit a resonant character at two different frequencies, non-harmonic of each other. Specific configurations for such cavity can be implemented to achieve a broadband light trapping that can be universally applied to increase photon absorption in any kind of thin film solar cell. When such cavity is applied to one of the top performing PV polymer blends (PTB7-Th: $PC_{71}BM$[34-36]), we demonstrate that we can achieve a power conversion efficiency (PCE) of 11.1%, corresponding to the highest power conversion efficiency ever measured for that polymer. The applicability of this new optical cavity is quite general and may be used, in

principle, to enhance the performance of any other thin film photovoltaic technology. Indeed, numerical estimates on the external quantum efficiency (EQE) made for perovskite cells indicate that such cavity is, at the moment, the only possible path to achieve a light energy harvesting capacity sufficient for the perovskite cells to reach their light harvesting limits.

2. Results and discussion

2.1 Two-resonance tapping cavity

A standard optical cavity, usually formed by a high reflectance mirror (HRM) separated a fixed distance from another partially reflecting metallic cavity layer (MCL), can be made to resonate at a fundamental frequency and its harmonics. The separation between the MCL and the HRM combined with the refractive index of the filling material univocally determines such cavity fundamental resonant frequency. In here, by adding a dielectric cavity layer (DCL) we obtain a cavity that when decreasing the MCL thickness can be made to resonate at a new fundamental frequency lying in between the fundamental and the second harmonic of the MCL optical cavity. Although such DCL sits at approximately the same distance the MCL is from the HRM, the boundary conditions for the electromagnetic field change drastically because the material changes from being a good quality conductor to a dielectric material. For a DCL cavity without a MCL, the boundary conditions are such that on the HRM side the resonant electrical field tends to vanish while on the DCL side the field amplitude takes a maximum value as seen in the top part of **Figure 1**a. When the MCL thickness is increased, at resonance the electrical field tends to vanish on both sides of the cavity, as seen in the bottom part of **Figure 1**a. The former case is similar to the vibration of string fixed from one end and loose from the other one, while the latter one is similar to the vibration of a string fixed from both ends. Indeed, the confinement capacity provided by such two non-harmonic resonances could be achieved with any type of wave provided the boundary conditions set are

similar to the ones that can be achieved when using the DCL and MCL combination. The difference in the boundary conditions is what allows to have two cavities with a very similar length and filled with the same index material, but resonating at two relatively close frequencies which are not subsequent harmonics of each other. When both the DCL and MCL are present and their thicknesses are fixed to some specific values that will be given below, the resulting cavity is non resonant at either one of the two frequencies, but at the same time light propagation within it has a reminiscence from both resonant frequencies. Light propagation in such new cavity we propose is analogous to the several cycles inharmonic vibration of a string during the transition of a note tapped by the right hand sustained or pulled off into a note fretted by the left hand in the two-handed tapping guitar playing technique. This is why, in what follows, we will refer to this new optical cavity as the two-resonance tapping cavity (TRTC).

When a TRTC is formed with the DCL adjacent to the MCL by increasing the thickness of the latter layer from zero to any value above 10 nm one can switch the resonance from the DCL to the MCL fundamental frequencies, as seen in **Figure 1**b. For intermediate MCL thicknesses, between 5 and 10 nm approximately, the field confinement effect from both fundamental resonances is smeared but the character from both resonances survives leading to a broadband light trapping. Note that this is fundamentally different than an anti-reflection coating that relies on achieving a high transmission via an optimal electromagnetic interference. The effectiveness in the light confinement provided by such TRTC is demonstrated by the observation of an increased light absorption. We consider a simple thin film solar cell configuration where the absorber material is a semiconductor exhibiting a square root growth for the density of states in terms of the excitation energy above the band gap. As seen in **Figure 1**c, for such type of material light collection can be, for certain sizes of the absorber layer, more than 2.5 mA/cm^2 larger for the two-resonance tapping cavity (TRTC)

configuration than for the standard cell configuration. The calculated external quantum efficiencies (EQE) when the material is a 100 nm thick PTB7-Th:$PC_{71}BM$ polymer blend layer or a larger than 600 nm thick methylammonium lead halide perovskite layer are shown in **Figure 1**d. One sees that the TRTC has the effect of increasing the EQE for wavelengths from the visible to near infrared spectrums. For perovskite cells the EQE, was computed based on a very accurate determination of its optical constants as detailed in section 1 of the Supporting Information file (Figure. S1-S4 and Table S1). It is worth noting that for the perovskite TRTC cell the predicted EQE approaches the internal quantum efficiency (IQE) for a wavelength range larger than 300 nm, covering almost entirely the useful absorption spectrum of such material.

2.2 Materials and architectures for a TRTC in a polymer cell

Several issues in the fabrication of a cavity compatible with the fabrication procedure of perovskite cells must be resolved before the TRTC can be implemented for such type of material. In the current work, we consider the implementation of the TRTC using a PTB7-Th:$PC_{71}BM$ polymer blend as absorber layer. Such absorber layer is enclosed in between a 100 nm thick Ag layer as HRM and the DCL and MCL. The latter one consisting of a 10 nm thick Ag layer sandwiched between two 5 nm ZnO layers. Although neither of the two ZnO layers play any relevant optical role, the bottom one is needed to optimize the transmission and electrical properties of the thin Ag layer, while the top one prevents any Ag degradation in the event that such electrode is exposed to the ambient air.[37-42] For the DCL, adjacent to the bottom ZnO layer, we considered four different dielectric materials with high transparency in the visible region of the spectrum: Al_2O_3, ZnO, MoO_3 and TiO_2. As can be seen in **Figure 2**a, a maximum short circuit current (J_{sc}) is predicted for the higher refractive index materials such as the TiO_2 or MoO_3. The optimal DCL thickness must be selected in each case to maximize the short circuit current in accordance to **Figure 2**a. As expected, when the

refractive index of the DCL (given in Supporting Information, Figure S5) increases, the resonance corresponding to that layer becomes sharper (see Figure S6, Supporting Information). When this is combined with a 10 nm Ag thickness for the MCL, one achieves a remarkable two-resonance tapping effect for the MoO_3 and TiO_2 cases. As seen in **Figure 2**b, in both cases, the MCL or DCL fundamental resonances are smeared and become barely distinguishable. In contrast, the standard resonant cavity formed without the DCL layer exhibits the usual single sharp resonance (see Figure 2b).

2.3 Light confinement and absorption in a TRTC polymer cell

To evaluate what effect does the predicted confinement, shown in **Figure 2**b, have on the light absorption by the polymer blend, we numerically computed and experimentally measured the EQEs of completed cells. The device architecture of fused silica substrate/DCL/ZnO (5 nm)/MCL/ZnO (5 nm)/SG-ZnO (10 nm)/PTB7-Th: $PC_{71}BM$ (95 nm)/MoO_3 (5 nm)/Ag (100 nm) was used for all the EQE experimental measurements. All DCL and MCL materials were deposited by magnetron sputtering at room temperature. Details are given in methods section. The exact thicknesses for each DCL layer (given in Table S2, Supporting Information) was determined numerically using the transfer matrix model outlined in the optical simulation section in Figure S7 in the Supporting Information. We used an inverse integration approach to find the cell configuration that maximizes the Jsc. The EQEs shown in Fig. 2c, as well as the J_{sc} values given in Table 1, clearly indicate that the TRTC obtained when the material of the DCL is either MoO_3 or TiO_2 leads to a broadband absorption. EQEs indicate a strong absorption in the green-red spectral regions for all cases, extending to the blue region when the refractive index of DCL material is larger. The optimal performance of the TRTC solar cell is found by adjusting the DCL as well as the MCL thickness as shown in **Figure 3**. As seen in **Figure 3**a, an almost wavelength independent EQE covering the entire absorption band of the PTB7-Th: $PC_{71}BM$ blend is found for a 19 nm

TiO_2 DCL. Similarly, if the contribution to the optical resonance of the MCL is diminished by reducing the Ag layer thickness within the MCL, one observes, as seen in **Figure 3**b, that the EQE is reduced in the green to near IR range of the spectrum.

2.4 Design of high efficiency PTB7-Th: $PC_{71}BM$ cells incorporating a TRTC

For an optimal light harvesting in a TRTC cell we reduced light reflection at the substrate by introducing an anti-reflection coating (ARC). The entire architecture of the corresponding solar device is shown in **Figure 4**a. As mentioned above, in the actual implementation of the TRTC two additional ZnO layers must be included. As can be seen in Figure. S8, the optical effect of such layers is to slightly reduce the field confinement capacity provided by either the DCL or the MCL cavities. However, as seen in Figure S8a when the MCL thickness is zero, a resonance at the blue ($\lambda \sim 440$ nm) side of the spectrum is clearly visible as in the top part of Figure 1a. On the other hand, when the thickness of the MCL is increased to 15 nm the resonance on the red ($\lambda \sim 655$ nm) side of the spectrum becomes apparent as seen in Figure S8b.

To determine the thickness for all layers, as well as the optimal index for the substrate we used a modified transfer matrix approach (see section 2 in Supporting Information) that combines the coherent superposition of field amplitudes within the ARC and cell layers with the superposition of field intensities within the substrate layer. Using this modified transfer matrix approach we numerically determined the maximum J_{sc} to be close to 18.9 mA/cm^2 for the following architecture: MgF_2 (100 nm)/N-SK10 substrate/DCL/ZnO(5 nm)/MCL/ZnO(5 nm)/SG-ZnO(10 nm)/PTB7-Th: $PC_{71}BM$ (95 nm)/MoO_3 (5 nm)/Ag (100 nm). Here DCL and MCL are made of 19 nm thick TiO_2 and 10 nm thick Ag, respectively. As noted above the contribution from the MCL and DCL resonances is smeared when the Ag thickness is in the 5 to 10 nm range. The combined effect of the wavelength dependence in the solar spectrum and

in the blend absorption pushes the optimal cell architecture towards a 10 nm thick MCL, favouring the MCL resonance over the DCL. But as seen in Figure S8c and **Figure 3**a the contribution from both resonances is clearly present in the optimal configuration. The TRTC cells, with or without the ARC, exhibit a higher J_{sc} than the ITO cell as can be seen in **Figure 4**b. With the TRTC the averaged PCE increases from 9.33% (reference ITO cell) to 10.62% and further increases to 11.01% when the ARC is incorporated. The increase in PCE here mainly originates from the enhancement in J_{sc} that jumps by more than 2 mA/cm^2 from 16.53 mA/cm^2 to 18.74 mA/cm^2 as shown in Table 2. Note that the enhancement in J_{sc} is achieved without sacrificing FF and V_{oc}. Indeed, as seen in Table 2 the TRTC devices exhibited higher FFs than ITO counterparts mainly due to a reduced average series resistance. This is consistent with a lower sheet resistance of 5.4 Ω/sq in the MCL based electrodes as compared to 15 Ω/sq for the ITO electrode. The J_{sc} distributions shown in Figure 4c demonstrate the reliability and reproducibility of the J_{sc} enhancement provided by the TRTC. The PCE and PV parameters of high-performance devices were independently tested at Newport laboratory that certified a PCE of 10.4 ± 0.23% (Figure S9, Supporting Information). Top PCEs can be obtained irrespective of the polymer blend used as can be seen in Figure S10 in the Supporting Information and PV parameters are summarized in Table S3, where PTB7-Th was substituted by the Poly[[4,8-bis[(2-ethylhexyl)oxy]benzo[1,2-b:4,5-b']dithiophene-2,6-diyl][3-fluoro-2-[(2-ethylhexyl)carbonyl]thieno[3,4-b]thiophenediyl]] (PTB7) or Poly[N-9'-heptadecanyl-2,7-carbazole-alt-5,5-(4',7'-di-2-thienyl-2',1',3'-benzothiadiazole)] (PCDTBT) polymer.

When comparing the EQE of the three cells shown in **Figure 4**d, we observe that the TRTC leads to an enhancement in the photon absorption for almost the entire wavelength range except at shorter wavelengths where the absorption of the materials used in MCL and/or in DCL is larger than the absorption of ITO. In addition, the EQE profile for both TRTC cases is

slightly higher towards the IR rather than the UV side. Although the TRTC can provide an almost wavelength independent flat photon absorption, this changes when the TRTC is designed to optimize the performance of a solar cell. In other words, the larger sun photon flux in the 700 to 800 nm range combined with the PTB7-Th: $PC_{71}BM$ absorption leads the inverse numerical optimization targeting the maximum J_{sc}, to yield an EQE that prioritizes an IR shifted photon absorption. Note that all EQEs were previously computed using the inverse integration approach to maximize J_{sc} (See Figure 4d) and, once the entire layer architecture was known, fabrication of the devices was carried out.

3. Conclusions

In this work, we demonstrate that we can construct an optical cavity to reach an optimal confinement for broadband electromagnetic waves. Contrary to the common believe that dielectric layers would act as simple anti-reflection coatings, we demonstrate that the combination of an insulator with a good conductor leads to the formation of an optical cavity that can be made to have a resonant character at two non-harmonic frequencies. The increase in energy storage capacity relies, precisely, in the inharmonicity of the electromagnetic field propagation within such cavity. We demonstrate that the energy confinement capacity seen remains even when the material composition is changed or the thickness of the active layer is increased, and can, in principle, be applied to reach efficiency limit performances for any kind of thin film photovoltaic device. The effect is, however, more pronounced, for materials where the absorption band of the photoactive material exhibits a large wavelength dependent absorption such as, for instance, in organic or metal halide perovskites. We demonstrated a record efficiency for the PTB7-Th polymer cell and predicted that in the event that the TRTC concept is applied to a standard perovskite cell the EQE would closely matched the IQE for a broad range of frequencies. Finally, the unique energy storage capacity of the TRTC concept,

that relies not on material properties but on the different boundary conditions that correspond to the use of a dielectric or metallic layer, is not limited to light and can be extended to the storage of other forms of energy carried by any kind of vibration or sound.

4. Experimental Section

Materials and solution preparation: The polymer PTB7-Th (Batch No. YY7096, purchased from 1-material), and $PC_{71}BM$ (purity > 99%, American Dye Source) were used as received without further purification. 2-inch diameter Al_2O_3, MoO_3, ZnO, TiO_2 and Ag targets from Kurt J. Lesker Company were used as received. 0.15 M of sol-gel ZnO (SG-ZnO) precursor solutions were prepared by dissolving zinc acetate dihydrate (Sigma-Aldrich, 200 mg) and ethanolamine (Sigma-Aldrich, 56 mg) in 2-methoxyethanol (Sigma-Aldrich, 6 mL) and this solution was vigorously stirred at 60 ^{o}C for 2 hours to complete the hydrolysis reaction in air and then stirred at room temperature for at least 12 hours. Solutions of PTB7-Th: $PC_{71}BM$ (1.0:1.5 by weight) with a total concentration of 25 mg/mL were prepared in chlorobenzene and stirred at 60 ^{o}C overnight in N_2-filled glovebox and additive 1, 6-Diiodohexane (DIH, 3.5% by volume) was added one hour prior to spin-coating.

ARC deposition: A 100 nm MgF_2 ARC layer was deposited on the pre-cleaned N-SK10 glass substrates via thermal-evaporation in vacuum ($< 5\times10^{-6}$ mbar) at a deposition rate of 0.5 Å/s. The thicknesses was monitored using a quartz crystal oscillator during deposition and later verified with a profile meter.

TRTC fabrication: DCL and MCL were fabricated on pre-cleaned fused silica (n=1.45) or N-SK10 (n=1.62) glass substrates by magnetron sputtering (Aja International Inc.) at room temperature. The sputtering chamber was initially evacuated to a base pressure of ~10^{-6} mtorr. The target-to-substrate distance was maintained at 30 cm and the holder was rotated at a speed of 60 rpm. TiO2 and ZnO were deposited in a pure Ar atmosphere, while Al_2O_3, MoO_3 and

Ag were deposited in a mixture of Ar/O_2 with flux ratios of 20:5.3, 6:20 and 20:1, separately. TiO_2 and ZnO targets were used to deposit the TiO_2 and ZnO films using a RF power of 80 W and 50 W, respectively. Al and Mo targets were used to deposit Al_2O_3 and MoO_3 films using the same DC power of 150W. The fabrication of the MoO_3 layers was also assisted by RF bias of 50W. An Ag target was used to deposit thin Ag layer on the top of ZnO seed layer in DC power of 18 W. The deposition rate was 0.05 Å/s, 0.11 Å/s, 2.0 Å/s, 0.26 Å/s and 0.67 Å/s for TiO_2, ZnO, Al_2O_3, MoO_3 and Ag, respectively. All the layers were grown at 3 mtorr and the fabrication process for each DCL/ZnO/MCL/ZnO was carried out without breaking the vacuum chamber.

Solar cell fabrication: Solar cells were fabricated by spin-casting SG-ZnO precursor on the as-prepared sputtered DCL/ZnO/MCL/ZnO and pre-cleaned patterned ITO (Lumtec, 15 Ω/sq) glass substrates. The sol-gel ZnO films were annealed at 150 ^oC in air for 20 min to form ca. 10 nm electron extraction layers. The prepared samples were then transferred into a N_2-filled glove box for spin-coating PTB7-Th: $PC_{71}BM$ blends with controlled thickness of 95 nm. The resulting photoactive films were dried in vacuum ($< 5\times 10^{-6}$ mbar) for at least one hour. Finally, MoO_3 (5 nm, 0.5 Å/s) and Ag (100 nm, 1 Å/s) were sequentially deposited on the top of photoactive layer through a shadow mask by thermal evaporation in vacuum of $< 5\times 10^{-6}$ mbar. The solar cell area is 0.12 cm^2. Solar cells were encapsulated with pre-cleaned glass slides using a UV-curable epoxy (DELO, LP655,) in N_2-filled glovebox before measuring in air.

Characterization and measurements: The solar cells were measured under a 1 sun, AM 1.5G spectrum from a solar simulator (ABET Sol3A, 1000 W/m^2). A Keithley 2420 was applied to measure the *J*–V characteristics in air. The illumination intensity of the light source (Xenon lamp, 300W, USHIO) was determined using a Hamamatsu silicon photodiode (with KG-5 filter, area = 0.1296 cm^2) certificated by ISE Fraunhofer. Spectrally resolved EQEs were measured using a bench top QEX10 Quantum Efficiency Measurement System (PV

Measurements). The electrical properties of the TRTC films were measured using four-point probe method. The transmission and reflectance spectra (Figure S11, Supporting Information) were recorded using an ultraviolet–vis–near-infrared spectrophotometer (Lambda 950, PerkinElmer).

Supporting Information

Supporting Information is available from the Wiley Online Library or from the author.

Acknowledgements

Q.L. and P.R.-G. contributed equally to this work. The authors acknowledge financial support from the Spanish MINECO (Severo Ochoa program, grant No.: SEV-2015-0522), the MINECO and the Fondo Europeo de Desarrollo Regional FEDER (grant No.: MAT2014-52985-R), the Fundació Privada Cellex, and from the EC FP7 Program (ICT-2011.35) under grant agreement n° NMP3-SL-2013-604506, Q. L acknowledges Erasmus Mundus doctorate program Europhotonics (Grant No. 159224-1-2009-1-FR-ERA MUNDUS-EMJD)

Received: ((will be filled in by the editorial staff))
Revised: ((will be filled in by the editorial staff))
Published online: ((will be filled in by the editorial staff))

Reference

[1] Q. Lin, A. Armin, R. Nagiri, P. Burn and P. Meredith, *Nat. Photonics* **2014**, 9, 106.

[2] R. A. J. Janssen and J. Nelson, *Adv. Mater*. **2013**, 25, 1847.

[3] B. Yang, O. Dyck, J. Poplawsky, J. Keum, A. Puretzky, S. Das, I. Ivanov, C. Rouleau, G. Duscher, D. Geohegan and K. Xiao, *J. Am. Chem. Soc*. **2015**, 137, 9210.

[4] T. Liu, K. Chen, Q. Hu, R. Zhu, Q. Gong, *Adv. Energy Mater*.**2016**, *6*,1600457

[5] D. Wang, H. Cui, G. Hou, Z. Zhu, Q. Yan and G. Su, *Sci. Rep*. **2016**, 6, 18922.

[6] Z. Tang, W. Tress and O. Inganäs, *Mater. Today,* **2014**, 17, 389-396.

[7] L. Dou, J. You, Z. Hong, Z. Xu, G. Li, R. Street and Y. Yang, *Adv. Mater.* **2013**, 25, 6642.

[8] C. Small, S. Tsang, S. Chen, S. Baek, C. Amb, J. Subbiah, J. Reynolds, F. So, *Adv. Energy Mater.* **2013**, 3, 909.

[9] M. L. Brongersma, Y. Cui and S. Fan, *Nat. Mater*. **2014**, 13, 451.

[10] Z. Tang, A. Elfwing, J. Bergqvist, W. Tress, O. Inganäs, *Adv. Energy Mater*. **2013**, 3, 1606.

[11] D. Ko, J. Tumbleston, L. Zhang, S. Williams, J. DeSimone, R. Lopez and E. Samulski, *Nano Lett*. **2009**, 9, 2742.

[12] Y. Liu, C. Kirsch, A. Gadisa, M. Aryal, S. Mitran, E. Samulski and R. Lopez. *J. Phys. D: Appl. Phys*. **2013**, 46, 024008.

[13] Y. Hsiao, F. Chien, J. Huang, C. Chen, C. Kuo, C. Chu and P. Chen, *J. Phys. Chem. C,* **2011***,* 115, 11864.

[14] M. Adachi, A. Labelle, S. Thon, X. Lan, S. Hoogland and E. Sargent, *Sci. Rep.* **2013**, 3, 2928.

[15] A. Mihi, F. J. Beck, T. Lasanta, A. K. Rath and G. Konstantatos, *Adv. Mater.* **2014**, 26, 443.

[16] S. Na, S. Kim, J. Jo, S. Oh, J. Kim and D. Kim, *Adv. Funct. Mater.* **2008***,* 18, 3956.

[17] K. S. Nalwa, J. M. Park, K. M. Ho and S. Chaudhary, *Adv. Mater*. **2011**, 23, 112.

[18] X. Yu, X. Yu, J. Zhang, Z. Hu, G. Zhao and Y. Zhao, *Sol. Energ. Mater. Sol. Cells,* **2014**, 121, 28.

[19] S. Colodrero, A. Mihi, L. Häggman, M. Ocaña, G. Boschloo, A. Hagfeldt and H. Míguez, *Adv. Mater.* **2009**, 21, 764.

[20] R. Betancur, P. Romero-Gomez, A. Martinez-Otero, X. Elias, M. Maymó and J. Martorell, *Nat. Photonics,* **2013**, 7, 995.

[21] F. Pastorelli, P. Romero-Gomez, R. Betancur, A. Martinez-Otero, P. Mantilla-Perez, N. Bonod and J. Martorell, *Adv. Energ. Mater*. **2015**, 5, 1400614.

[22] W. Yu, X. Jia, Y. Long, L. Shen, Y. Liu, W. Guo and S. Ruan, *ACS Appl. Mater. Interfaces*, **2015**, 18, 9920.

[23] C. Bronnbauer, N. Gasparini, C. J. Brabec and K. Forberich, *Adv. Optical Mater.* **2016**, 4, 1098.

[24] R. Lunt and V. Bulovic, *Appl. Phys. Lett.* **2011**, 98, 113305.

[25] J. Grandidier, D. M. Callahan, J. N. Munday and H. A. Atwater, *Adv. Mater*. **2011**, 23, 1272.

[26] Y. Yao, J. Yao, V. Narasimhan, Z. Ruan, C. Xie, S. Fan and Y. Cui, *Nat. Commun*. **2012**, 3, 664.

[27] M. Mariano, F. J. Rodríguez, P. Romero-Gomez, G. Kozyreff, and J. Martorell, *Sci. Rep*. **2014**, 4, 4959.

[28] J. Wu, F. Chen, Y. Hsiao, F. Chien, P. Chen, C. Kuo, M. Huang, C. Hsu, *ACS Nano* **2011**, 5, 959.

[29] L. Lu, Z. Luo, T. Xu and L. Yu, *Nano Lett.* **2012**, 13, 59.

[30] X. Li, W. Choy, L. Huo, F. Xie, W. Sha, B. Ding, X. Guo, Y. Li, J. Hou, J. You and Y. Yang, *Adv. Mater.* **2012**, 24, 3046.

[31] X. Wang, H. Zhu, Y. Xu, H. Wang, Y. Tao, S. Hark, X. Xiao and Q. Li, *ACS Nano*, **2010**, 4, 3302.

[32] F. Pastorelli, S., Bidault, J. Martorell and N. Bonod, *Adv. Optical Mater.* **2014**. 2, 171.

[33] H. Choi, S. Ko, Y. Choi, P. Joo, T. Kim, B. Lee, J. Jung, H. Choi, M. Cha, J. Jeong, I. Hwang, M. Song, B. Kim and J. Kim, *Nat. Photonics* **2013**, 7, 732.

[34] S. H. Liao, H. J. Jhuo, Y. S. Cheng and S. A. Chen, *Adv. Mater*. **2013**, 25, 4766.

[35] Z. He, B. Xiao, F. Liu, H. Wu, Y. Yang, S. Xiao, C. Wang, T. Russell and Y. Cao, *Nat. Photonics* **2015**, 9, 174.

[36] Q. Liu, P. Mantilla-Perez, M. Montes Bajo, P. Romero-Gomez and J. Martorell, *ACS Appl. Mater. Interfaces* **2016**, 8, 28750.

[37] N. Sergeant, A. Hadipour, B. Niesen, D. Cheyns, P. Heremans, P. Peumans and B. Rand, *Adv. Mater.* **2012**, 24, 728.

[38] J. Huang, C. Li, C. Chueh, S. Liu, J. Yu, A. Jen, *Adv. Energy Mater*. **2015**, 5, 1500406.

[39] W. Wang, M. Song, T. Bae, Y. Park, Y. Kang, S. Lee, S. Kim, D. Kim, S. Lee, G. Min, G. Lee, J. Kang and J. Yun, *Adv. Funct. Mater*. **2014**, 24, 1551.

[40] D. Ghosh, Q. Liu, P. Mantilla-Perez, T. Chen, V. Mkhitaryan, M. Huang, S. Garner, J. Martorell and V. Pruneri, *Adv. Funct. Mater*. **2015**, 25, 7309.

[41] S. Colodrero, P. Romero-Gomez, P. Mantilla-Perez and J. Martorell, *Adv. Funct. Mater*. **2017**, 27, 1602969.

[42] D. Zhao, C. Zhang, H. Kim, L. J. Guo, *Adv. Energy Mater*. **2015**, 5, 1500768.

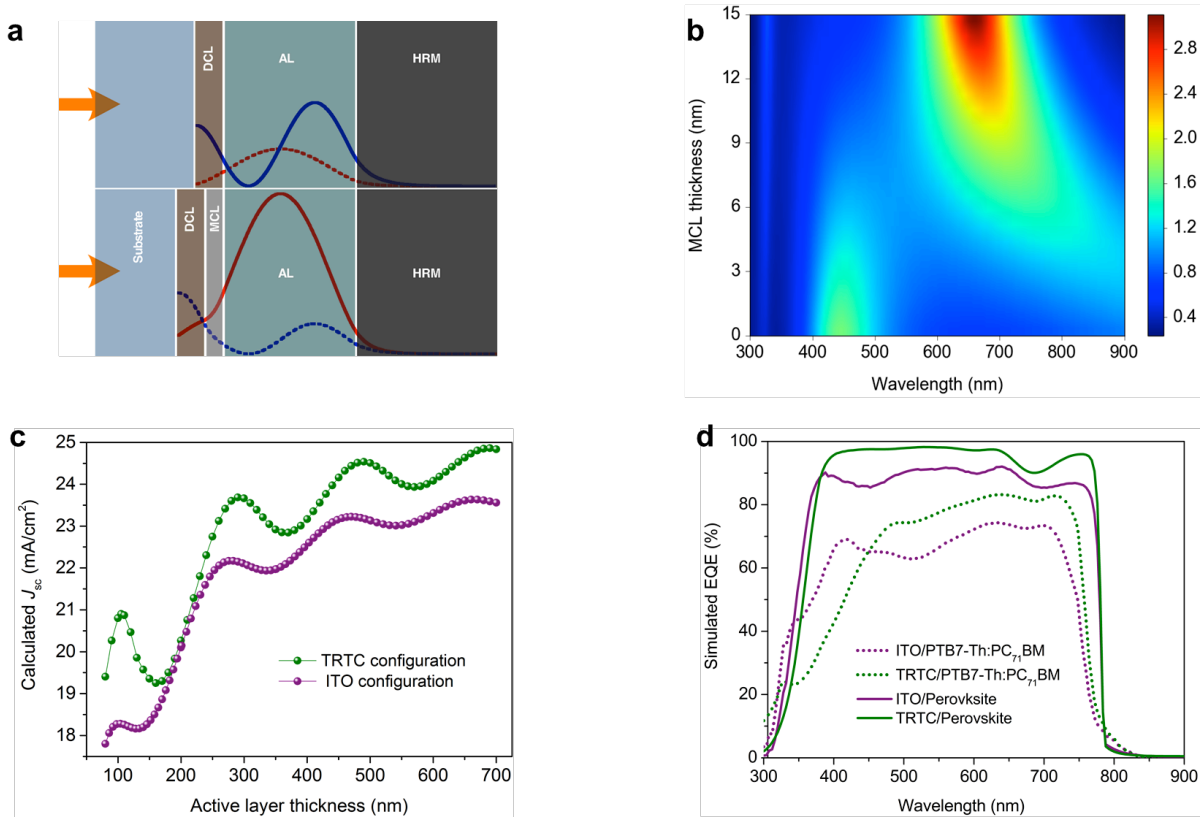

Figure 1. a) Schematic diagram of cavities formed by an AL dispersion less layer (n=2.0 and k=0) sandwiched in between a DCL and a HRM (top), and by an AL sandwiched in between a DCL/MCL and a HRM (bottom). Blue and red curves correspond to field intensity distributions at 440 nm and 655 nm, respectively. The resonant field intensities are shown as solid lines while the non-resonant ones are shown as dashed. b) Computed field amplitude in a dispersion less (n=2.0 and k=0) AL as a function of the wavelength and MCL thickness. The device architecture used was MgF_2 (94 nm)/N-SK-10 substrate/DCL (20 nm)/MCL (0-15 nm)/AL (107 nm)/Ag (100 nm). c) Predicted optimal short-circuit current as a function of the AL thickness when the material is a semiconductor in a standard ITO configuration cell (purple) or in TRTC configurations (olive). d) Simulated EQEs for PTB7-Th: $PC_{71}BM$ and perovskite cells in the standard ITO (purple) or in the TRTC (olive) configurations. The TRTC architectures used were for the polymer cell: MgF_2 (100 nm)/N-SK10 substrate/TiO_2 (19 nm)/ZnO (5 nm)/Ag(9.6 nm)/ZnO(5 nm)/SG-ZnO(5 nm)/PTB7-Th: $PC_{71}BM$ (96 nm)/MoO_3 (5 nm)/Ag (120 nm) and for the perovskite cell: MgF_2 (100 nm)/N-SK10 substrate/TiO_2 (22 nm)/ZnO (5 nm)/Ag (6 nm)/ZnO (5 nm)/NP-TiO_2 (42 nm)/Perovskite (619 nm)/Spiro-OMeTAD (100 nm)/Ag (100 nm). In all figures the materials for DCL and MCL are TiO_2 and Ag, respectively.

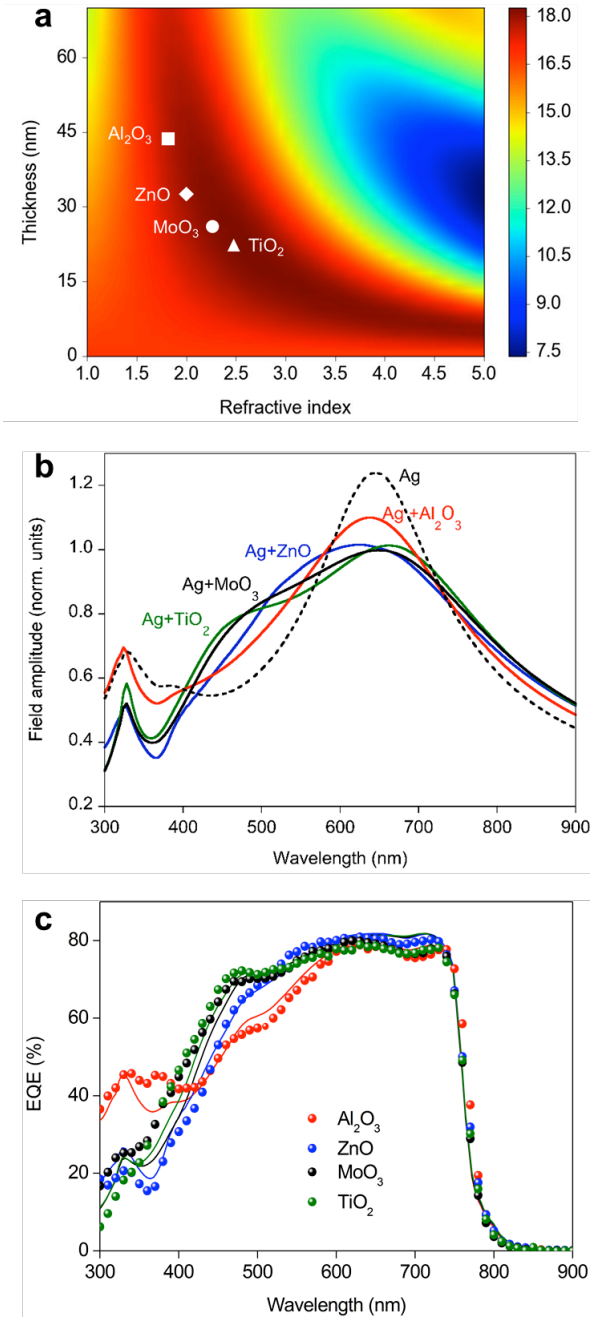

Figure 2. a) Numerically computed short circuit current as a function of DCL refractive index and thickness when the AL material was the PTB7-Th: $PC_{71}BM$ blend. The optimal DCL for the dielectric materials used in the experiments are indicated: Al_2O_3 (square), ZnO (diamond), MoO_3 (circle), and TiO_2 (triangle). IQE here for simulations is assumed to be 90%. b) Optical field amplitude in the AL layer as a function of the wavelength when the AL is a non-absorbing dielectric with a refractive index real part equal to 1.8 and the Ag MCL thickness is taken to be **1**0 nm, and the DCL materials are Al_2O_3 (red solid line), MoO_3 (black solid line), ZnO (blue solid line) and TiO_2 (green solid line). c) Experimentally measured (dots) and simulated (solid lines) EQEs for PTB7-Th:$PC_{71}BM$ cells based on the above four DCL materials with predicted optimal thickness.

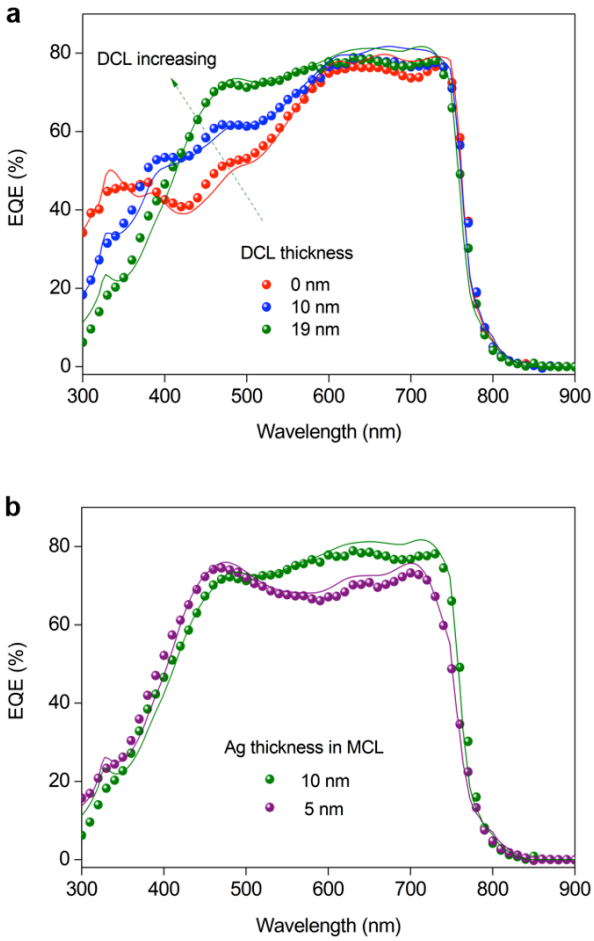

Figure 3. For the (Fused silica substrate)/DCL/ZnO(5 nm)/MCL/ZnO(5 nm)/SG-ZnO(10 nm)/PTB7-Th:$PC_{71}BM$(95 nm)/MoO_3(5 nm)/Ag(100 nm): Experimentally measured (dots) and computed (solid lines) EQEs when: a) The MCL is fixed to a 10 nm Ag layer and the DCL corresponds to a TiO_2 layer of 0 nm (red dots), 10 nm (dots), and 19 nm (green dots) in thickness. b) The DCL is fixed to a 19 nm TiO_2 layer and the MCL corresponds to a Ag layer with 5 nm (purple) and 10 nm (green) thickness.

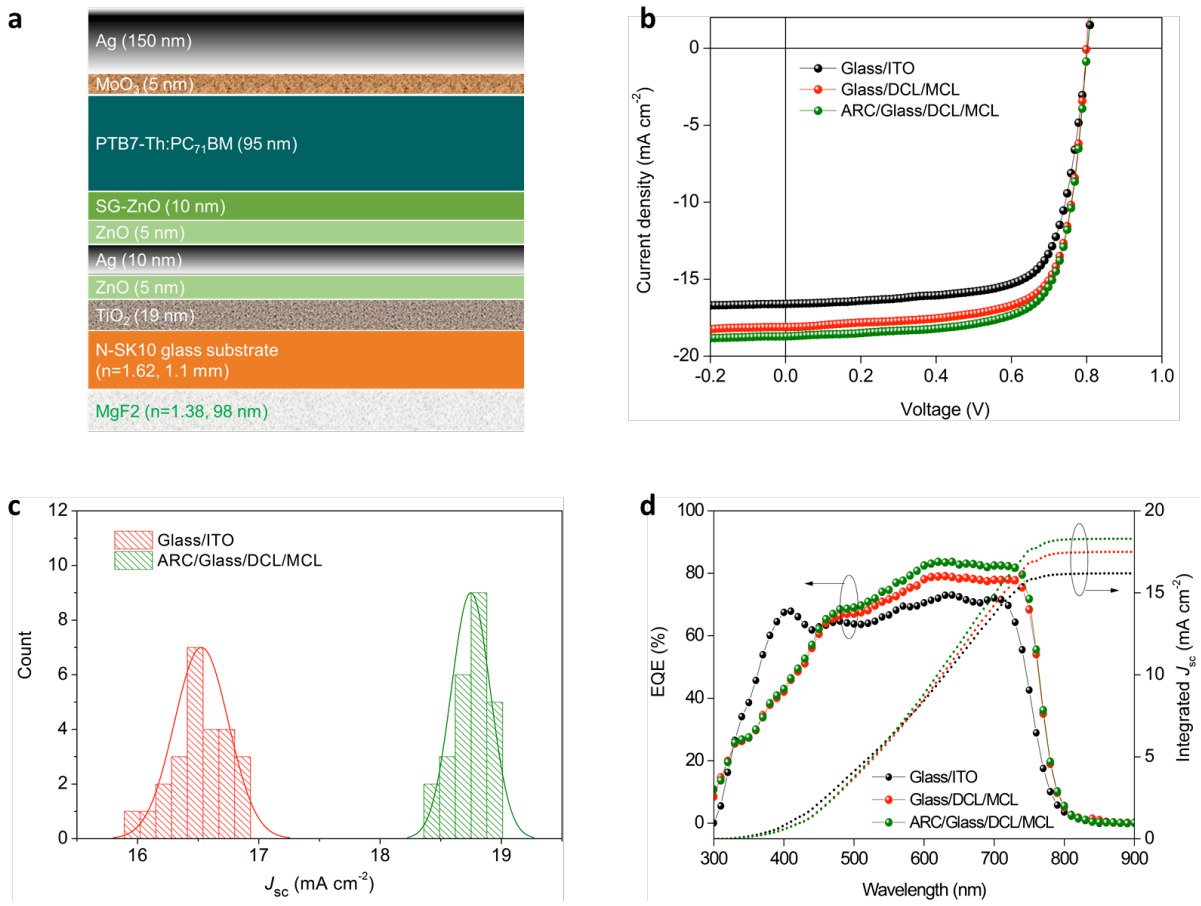

Figure. 4 a) Device layout for the optimal TRTC architecture incorporating an ARC. b) Current density-voltage (*J*-V) characteristics when measured under AM 1.5G illumination at 100 mW/cm^2. c) J_{sc} distribution for 25 ITO devices (red bars) and for 25 devices as in a) (green bars). The solid lines represent the Gaussian distribution fittings. d) Experimentally measured EQE and intergrated J_{sc} from EQE curves for an ITO cell on soda-lime (black), the cell in a) with (green) and without (red) the ARC.

Table 1. Photovoltaic properties of inverted PTB7-Th: $PC_{71}BM$ devices employing various TRTC configurations under AM 1.5G solar illumination at 100 mW cm^{-2}.

DCL material	Thickness (nm)	J_{sc} (mA cm^{-2})	V_{oc} (V)	FF (%)	PCE (%)
Al_2O_3	44	17.54 ± 0.25	0.800 ± 0.001	73.1 ± 0.4	10.25 ± 0.14 (10.43)
ZnO	33	17.96 ± 0.20	0.800 ± 0.001	73.4 ± 0.7	10.56 ± 0.09 (10.69)
MoO_3	26	18.29 ± 0.20	0.796 ± 0.001	73.2 ± 0.3	10.66 ± 0.10 (10.78)
TiO_2	19	18.45± 0.13	0.797 ± 0.001	72.9 ± 0.5	10.72 ± 0.11 (10.86)

Device structure here is fused silica substrate /DCL/ZnO (5 nm)/MCL/ZnO (5 nm)/SG-ZnO (10 nm)/AL (95 nm)/MoO_3 (5 nm)/Ag (100 nm) with MCL Ag (10 nm). 'Thickness' indicates DCL thickness; J_{sc}, short-circuit current; V_{oc} open-circuit voltage; FF, fill-factor; PCE, power conversion efficiency. The average values and standard deviations are obtained from over 10 devices and the value in the parentheses corresponds to the best devices.

Table 2. Photovoltaic parameters of ITO and TRTC based solar cells under AM 1.5G solar illumination at 100 mW cm^{-2}.

Cell configuration	J_{sc} (mA cm^{-2})	V_{oc} (V)	FF (%)	PCE (%)	Simulated J_{sc} (mA cm^{-2})	R_{series} (Ω)	R_{shunt} (kΩ)
Glass/ITO	16.53 ± 0.22	0.790 ± 0.006	71.1 ± 0.1	9.33 ± 0.16 (9.60)	16.74	64.3	18.7
Glass/DCL/MCL	18.09 ± 0.13	0.800 ± 0.002	73.3 ± 0.3	10.62 ± 0.11 (10.53)	18.32	31.0	21.3
ARC/Glass/DCL/MCL	18.74 ± 0.17	0.802 ± 0.002	73.0 ± 0.3	11.01 ± 0.09 (11.13)	18.90	32.1	23.8

ARC corresponds to MgF_2 (100 nm) while the DCL/MCL structure incorporates two ZnO layers is TiO_2 (19 nm)/ZnO (5 nm)/Ag (10 nm)/ZnO (5 nm). The average values and standard deviations are obtained from 25 devices and the best PCE values are shown in parentheses. Simulated J_{sc} are computed using a modified transfer matrix model assuming an internal quantum efficiency of 90%.

The table of contents.

A broadband two-resonance tapping cavity is proposed to effectively trap the light in the absorber layer in thin-film solar cells. When this new physical concept is applied to the polymer cells we fabricated, we reached the highest possible power conversion efficiency, corresponding to a 19% increase relative to an optimal reference cell.

Keywords: Thin-film solar cell, light trapping, optical cavity, PTB7-Th, Perovskite

Quan Liu,[1†] Pablo Romero-Gomez,[1†] Paola Mantilla-Perez,[1] Silvia Colodrero,[1] Johann Toudert,[1] and Jordi Martorell[1, 2]*

Title: A two-resonance tapping cavity for an optimal light trapping in thin-film solar cells